Debye screening, over-screening and specific adsorption in solutions of organic ions †

Fernando Bresme*[a,b], Oliver Robotham[a], Weng-I Katherine Chio[a], Miguel Angel Gonzalez[a,c] and Alexei Kornyshev[a]

Tetrabutylammonium (TBA) and Tetraphenylborate (TPB) ions dissolved in dichloroethane (DCE) are widely used in electrochemistry of liquid-liquid interfaces. Unlike alkali halide solutions in water, TBA-TPB-DCE solution feature large organic ions and a solvent with a dielectric constant almost one order of magnitude lower than that of water. This is expected to dramatically amplify the impact of ionic correlations in the properties of the solution. Here we report atomistic simulations of TBA-TPB-DCE solutions and analyze ion correlations, clustering, and charge screening effects. We target concentrations in the range 0.01-0.25 molal (m), hence exploring concentration regimes typical for many experimental investigations. We show that the transition from monotonic to oscillatory decay of the charge density, which signals the onset of strong ion correlations, takes place in this concentration interval, leading to over-screening effects. Furthermore, we investigate the distribution and adsorption of ions at the DCE-air interface. Unlike what is observed for small inorganic ions in water at similar concentrations, we find that TPB and TBA ions accumulate near the DCE surface, resulting in significant interfacial clustering and adsorption at concentrations $\sim$ 0.25 m. TPB ions adsorb more strongly leading to free energy wells of $\sim$ 1-2 k_BT. The adsorption modifies significantly the electrostatic potential of the DCE-air interface, which undergoes a shift of 0.2 V in going from pure DCE to TBA-TPB-DCE solutions at 0.25 m.

1 Introduction

Electrolytes play a key role regulating charge screening of colloids and biomolecules. Further they provide leverage for controlling electrochemical reactions and energy storage. The theory of aqueous solutions was tackled early on by Debye and Hückel who set up a successful mean field approach that is still widely used at low concentrations, and that serves as a robust reference to measure non-ideal behavior, *e.g.* associated to ion correlations, which can manifest itself in the formation of clusters and over-screening[1]. The interaction of ions at interfaces is also of considerable interest in atmospheric chemistry and electrochemistry. Onsager and Samaras theory[2] and its modifications[3] provided a simple interpretation of the increase of surface tension with salt concentration in simple electrolytes.The early interpretation of ion activity at interfaces was refined over the years, and more recently it has been shown that ions can accumulate at interfaces[4–6]. Such accumulation is not in contradiction with overall negative adsorption, as predicted by the Gibbs adsorption isotherm[7].

The study of bulk aqueous solution has witnessed a revival due to the recent reports of under-screening effects[8,9], experimentally observed in solutions of alkali halides at high concentrations, $>$ 1 M, and under confinement conditions, showing there are still outstanding questions in the area of electrolyte solution that challenge the predictions of well established theories.

In comparison with aqueous solutions, the theoretical investigation of organic ions has received less attention. However, these solutions feature in a number of systems of crucial importance in electrochemistry of liquid-liquid interfaces, such as "Interface between Two Immiscible Electrolyte Solutions" (ITIES). Such interfaces involve aqueous solutions in contact with an organic solvent containing, *e.g.* fatty organic ions. As reviewed before[10,11], ITIES encompass a wide range of applications, such as phase-transfer-catalysis or photochemical energy conversion. More recently, ITIES have been successfully employed to trap metallic nanoparticles in two dimensional arrays, enabling the design of self-assembled tuneable nanoplasmonic optical metasurface mirrors[12–14]. The accuracy of mean field approaches (Gouy-Chapman) to describe ion distribution at these interfaces has been addressed recently, and the structure of the interface examined using x-ray reflectivity[15]. The latter technique is particularly powerful to study the interfacial structure, albeit some of the organic ions used in the organic phase do not always of-

[a] *Department of Chemistry, Imperial College London, White City Campus, 80 Wood Lane, London W12 0BZ, UK. Tel: +44 (0)207 594 5886; E-mail: f.bresme@imperial.ac.uk*

[b] *Department of Chemistry, Norwegian University of Science and Technology, Trondheim, Norway*

[c] *Present Address, Departmento de Química Física I, Universidad Complutense de Madrid, Madrid, Spain*

† Electronic Supplementary Information (ESI) available

fer enough contrast to provide a full resolution of the interface. The adsorption of ions at the interface has also been tackled, approaching the infinite dilution limit, using computer simulations. The information emerging from these simulations was discussed with reference to the reflectivity experiments[7].

Ionic solutions in organic solvents have similarities with alkali halide aqueous solutions. The most obvious and generic one is the presence of charges dispersed in a polar solvent. However, organic solvents bring new challenges, which arise from their much lower dielectric constants, as compared with water, and the much larger size of the ions, as compared with alkali halides. As a matter of fact, tetraphenylborate (TPB) and tetrabutylammonium (TBA) ions consists of about 20 atoms, and they have diameters of the order of 1 nm, as compared with 0.2-0.4 nm for alkali halides. These differences bring a number of questions we would like to address: how do the organic ions distribute themselves in the solvent? How relevant are dispersion interactions? The latter are expected to be much more important than in *e.g.* alkali halide solutions. How do these interactions influence the structure of the solution, and the onset of over-screening? And ultimately, of specific relevance to ITIES, how do these interactions affect the interfacial structure, and how much interfacial adsorption is present? To tackle some of these questions we have performed atomistic simulations of a prototypical solution used in ITIES consisting of tetraphenylborate and tetrabutylammonium ions in 1,2-dicholoroethane. We target a wide range of concentrations from 0.01 molal to 0.25 molal (m), and examine the structure, screening and interfacial behavior of the ions, thus bringing light on the microscopic properties of these solutions.

Our article is structured as follows. Firstly, we describe the simulation approach and forcefields employed in this work. A discussion of our main results for bulk and interfaces follows. We close our paper discussing the main conclusions arising from our work.

2 Methods

We performed atomistic simulations of tetraphenylborate (TPB) and tetrabutylammonium (TBA) ions in 1,2-dicholoroethane (DCE). All the simulations reported here were performed at 298 K and 1 bar pressure for bulk systems, and coexistence pressure for the simulations of the DCE-air interfaces. The bulk simulations were performed with 8 or 64 ion pairs dissolved in 7104 or 2584 DCE molecules to achieve target concentrations varying between 0.01 and 0.25 molal (m). The equation of state of the solution was obtained from simulations at constant temperature and pressure using the v-rescale thermostat[16] (coupling constant 1 ps) and the Berendsen barostat[17] (coupling constant 2 ps and compressibility 4.5×10^{-5} bar^{-1}). Dispersion and electrostatic interactions were computed in full using the Particle Mesh Ewald method[18]. A typical simulation involved an equilibration of 1 ns and a production time spanning at least 40 ns, using a timestep of 2 fs. The simulations of the DCE and DCE/solution interfaces were performed using prismatic boxes with typical box lengths, $L_x = L_y = 7.45 - 9.99$ nm and $L_z = 25 - 50$ nm. These simulations were prepared by replicating 3 times boxes containing a previously equilibrated bulk liquid. Subsequently, a large vacuum region above and below the liquid slab was set, to allow the interface to form. The new configuration was equilibrated for 3 ns, following a production phase spanning 50 ns. The trajectories were used to obtain density profiles and surface tensions and used later to calculate the ion adsorption. The surface tension was obtained using the microscopic virial route, $\gamma = L_z(P_{zz} - 1/2(P_{xx} + P_{yy}))/2$ where $P_{\alpha\beta}$ are the components of the pressure tensor with P_{zz} defining the vapour pressure, and the factor of "2" takes into account that we are simulating a liquid slab and therefore two interfaces. The dielectric constant was obtained by computing the variance of the dipole moment of the whole (cubic) simulation cells, including all the charges present in the simulation box.

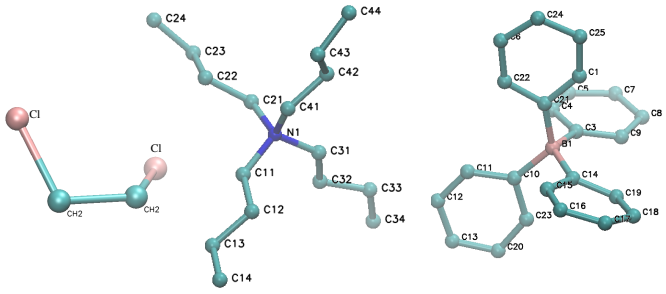

Fig. 1 Molecular models and atom types of DCE (Left), TBA (Middle) and TPB (Right). The atom numbers are used in the SI to define the different forcefields employed in this work.

The molecular structure of the solvent (DCE), the cation (TBA) and the anion (TPB) are shown in Figure 1. The tables in the supporting information (SI) compile the details of the forcefields employed in this work, with reference to the atom labels shown in this Figure. All the forcefields used here are based on the united atom approach. The parameters for DCE are based on the OPLS forcefield[19]. The bonds between pairs of atoms were modelled as rigid, while the angular interactions and dihedral interactions were modelled explicitly. A fudge factor of 0.5 was chosen to model the intramolecular dispersion and coulombic interactions. The intermolecular interactions were modeled using coulombic and Lennard-Jones potentials. Equations and numerical values for the forcefields parameters are reported in the tables in the SI. The partial charges on the CH_2 pseudoatoms and Cl atoms in DCE, were parametrized to reproduce the experimental dielectric constant and the density of the liquid at standard conditions (P=1 bar, T=298 K). It was found that these parameters also predict a surface tension at 298 K in good agreement with the experimental data.

The ions, TBA and TPB, were also modelled using the united atom approach. We used the ATB database[20] to select partial charges and topologies. The topology is based on PM3 (optimized geometry) and MOPAC (charges) for TBA, and B3LYP/6-31G* (optimized geometry) and the Merz-Kollman (charges) method for TPB. The parameters for the dispersion interactions are based on the GROMOS 53A6 forcefield[21]. We derived cross interactions between different atoms using geometric combination rules, both for the effective diameter and the interaction strengths. The tra-

jectories were generated with GROMACS[22] v 5.1.4.

3 Results

3.1 Bulk properties

We show in Table 1 the thermodynamic properties of DCE at standard conditions. The forcefield used here reproduces accurately the dielectric constant (within 0.1%), and the density and surface tension are within ∼2% and ∼9% of the experimental values, respectively. The addition of salt induces a reduction of the dielectric constant, similarly to the trends observed in aqueous solution of alkali halides, but the effect is significantly stronger for DCE, for the same ion concentrations. Indeed, for monovalent ions, experiments of *e.g.* NaCl solutions show that concentrations of the order of ∼0.1-0.3 m lead to a reduction of the dielectric constant of $\sim 1\%$ [23], while in our simulations of DCE solutions at 0.25 m concentration the reduction is already ~ 20 %. For the lower concentrations investigated here (~ 0.01 m) used in a wide range of electrochemical experiments, the dielectric constant is approximately the same as in pure DCE within the statistical error of the simulations.

The enhanced effect of TBA-TPB on the dielectric constant of the solution, as compared to aqueous solutions, is connected to approximately 8 times longer Bjerrum length in DCE than in water, and correspondingly to a much stronger dielectric saturation effect. Indeed, the described saturation length scale is useful to understand our results[24] . Following previous works[25] the quantity $l_h = \sqrt{l_b b}$ defines the thickness of the solvation layer around a given ion, such that the dipoles of the solvating molecules would be influenced by the ion electrostatic field. l_b is the Bjerrum length and b the dipole length. The Bjerrum length for our system at 298 K is ~ 5.6 nm, with a dipole length of $b \sim 0.05$ nm (using the dipole moment of 1,2-DCE in the gas phase), we estimate $l_h \sim$ 0.5 nm. This distance is likely to be even longer, as shown in the ion-solvent RDFs (see figure 2). Referring to the ion-solvent pair correlation function calculated for both TBA and TPB (see Figure 2), shows oscillations up to 1 nm distances from the center of mass of the ions.

At 0.25 m the average distance between ions (considering both cations and anions) is ~ 1.5 nm which is longer than l_h. However, the TBA and TPB ions are not point particles, their diameters are 3 times larger than e.g. Na^+, hence the surface to surface separation between ions is about $l_s s \sim 0.5$ nm, which is of the order of l_h giving a ratio $l_s s/l_h \sim 1$. This analysis shows that the overlap of the solvation layers around neighboring ions is indeed possible. Taking an intermediate value for $l_s s \sim 0.75$ nm instead, we get a ratio $l_s s/l_h \sim 1.5$, showing that at 0.25 m and considering inter-ionic overlap, the overlap of solvation layers is still possible. These calculations indicate that at a concentration of 0.25 m the solvation shells of the ions interact with each other.

For alkali halide aqueous solutions, such as NaCl, a reduction in the dielectric constant of 20% is observed at much higher concentrations, 1.5 m. A similar analysis at this concentration gives $l_s s/l_h \sim 1.5$, using $l_h \sim 0.5$ nm and $b = 0.1$ nm[26], as well as $l_s s \sim 0.75$ nm (considering the effective size of the ions ~ 0.3 nm and the average distance between the ions, ~ 0.8 nm. Hence the change in the dielectric constant observed for TBA-TPB solutions in DCE seems consistent with the expected decrease in aqueous electrolytes when accounting for the different Bjerrum length, ion size and characteristic length-scale of the solvation layer around the ions.

The diffusion coefficients of TBA and TPB decrease with salt concentration. The absolute values are smaller than the ones observed for inorganic alkali halides. This is expected given the larger diameters of the organic ions, ~ 1 nm *vs* 0.2-0.4 nm for alkali halides, respectively. Considering diffusion coefficients for alkali halides, $D_{Na} \sim 1.5 \times 10^{-9}$ m$^2/s$ and $D_{Cl} \sim 2 \times 10^{-9}$ m$^2/s$ the reduction in diffusion coefficient of cations, $D_{TBA,0.01m}/D_{Na} \sim 0.5$ and anions $D_{TPB,0.01m}/D_{Cl} \sim 0.35$ is compatible with the Stokes-Einstein equation, $\eta_{H_2O} r_{Na}/\eta_{DCE} r_{TBA} \approx 0.3$ and $\eta_{H_2O} r_{Cl}/\eta_{DCE} r_{TPB} \approx 0.4$, where $\eta_{DCE} = 0.8$ mPa s and $\eta_{H_2O} = 1$ mPa s, are the viscosities of DCE and water at 20^{o}C, respectively, and $r_{TBA} \approx r_{TBP} \sim 0.5$ nm, while $r_{Na} = 0.116$ nm and $r_{Cl} = 0.167$ nm are the radii of the alkali ions.

The density of the solution decreases with increasing salt concentration. This behavior is very different to that observed in many aqueous ionic solutions, where the volume of the solution contracts due to the on hydration and consequently the density increases with salt concentration. We expect that the reduction in the density observed here is connected to the larger size of the ions and their effective lower density, hence leading to an overall reduction of the density of the solution. The density dependence on concentration is one of the properties that distinguishes the TBA-TPB-DCE solution from a standard alkali halide solution.

We examine in Figure 2 the structure of the DCE solution. The structure varies significantly with the electrolyte concentration, and it is evident that in going from 0.01 to 0.1 m the ion correlations change from a monotonic varying function to an oscillatory one. The cation-cation (*cc*) and cation-anion (*ca*) pair correlations functions reveal the same behavior observed for simple spherical ions, with the observation of oscillations of the cc and ca RDF's in anti-phase at higher concentrations (see 0.1 and 0.25 m), which is characteristic of the structure observed in dense charged systems. Advancing the discussion below, we find that higher ion correlations give rise to over-screening, or local overcompensation of the charge of a given central ion, followed by an oscillatory decay of the screening charge with the radial distance. Such effects have been discussed before in studies of primitive models (non-explicit solvent and Brownian Dynamics) of aqueous solutions, although clear oscillations start there at much higher concentrations ~ 1 M[29]. This observation can be rationalised in terms of the transition from weak to strong electrostatic coupling, which in DCE should occur at lower electrolyte concentrations, due to the much larger Bjerrum length in the DCE solution. Hence, the transition to the oscillatory behavior and over-screening is observed at intermediate concentrations, while the decay is monotonic at the lower concentrations, 0.01 m, used often in electrochemical experiments. This observation supports the use of mean field approaches at these low concentrations and justifies the fact that the Verwey-Niessen theory[30] works well when describing capacitance measurements of interfaces of two immiscible electrolytic solutions.

Table 1 Thermodynamic and dynamic properties of pure DCE and DCE-TBA-TPB solutions as a function of salt concentration (molal). The density (ρ kg/m^3), dielectric constant (ε) and diffusion coefficients (D$\times 10^{-9}$ m^2/s) were computed at T=298 K and P=1 bar pressure. The diffusion coefficients were obtained from the analysis of the mean square displacement using Einstein's equation. The surface tensions (γ mN/m) were computed from simulations involving explicit interfaces at 298 K. c and $c_{int.}$ indicate the concentration of salt in the bulk simulations, and the concentration of salt (far from the DCE surface) in the interfacial simulations, respectively. Experimental data taken from: a[27] and from limiting ionic conductivities reported in b[28].

c	ρ	ε	D_{DCE}	D_{TBA}	D_{TPB}	$c_{int.}$	γ
0	1275.6±0.01	10.35±0.20	1.93±0.01			0	35.1±0.8
0.01	1271.5±0.03	10.3±0.1	1.93±0.02	0.69±0.18	0.70±0.16	0.008	35.7±0.8
0.05	1252.0±0.04	9.82±0.1	1.87±0.02	0.68±0.13	0.66±0.18		
0.1	1231.4±0.01	9.53±0.2	1.83±0.01	0.55±0.10	0.63±0.1	0.093	33.6±0.3
0.25	1170.8±0.04	8.22±0.1	1.63±0.01	0.53±0.05	0.48±0.05	0.21	32.9±0.9
0	1246.3[a]	10.36[a]	1.72[a]	0.74[b]	0.59[b]		31.5[a]

Unlike the *cc* and *aa* RDFs, the *ca* RDF features a more complex structure. The main peak of the *ca* RDF shows two sub-peaks, at 0.72 and 1.1 nm (see Figure 2). The sub-peaks indicate favourable distances for ion interactions, with the shorter distance corresponding to a preferred conformation of TBA and TPB, which results in better ion packing. A configuration showing the arrangement of the ions for these two distances is depicted in Figure 3. Examination of the simulation snapshots reveals the formation of clusters consisting of ions of alternating charge. This structure is reminiscent of that reported in simple models of electrolytes using the restricted primitive model (RPM)[31].

We computed the cluster size distribution, $P(s)$, by calculating the average number of clusters of size s using 1.1 nm as cut-off distance between the center of mass of the ions. All ions irrespective of their charge were included in order to construct the clusters. $P(s)$ is normalized, and therefore it is a probability distribution function. The mean cluster size was obtained from $\langle S\rangle = \sum_{s=1}^{s_m} sP(s)$, where s_m is the maximum cluster size.

For the DCE solutions the mean cluster size (see Table 2) reflects the formation of few "Bjerrum" pairs at the lower concentrations, 0.01 and 0.1 m, and larger clusters, involving more than two ions, at the higher concentrations (0.25 m). Snapshots of representative clusters formed in these solutions are shown in Figure 3. The cluster size distribution function features a monotonic decay with the cluster size, s. Such behaviour is consistent with that reported before for the RPM model[31]. To allow a direct comparison of our DCE solution with the RPM model, we calculate the density of ions in our system at 0.01 m concentation in terms of the reduced density of $\rho^* = (N/V)\sigma_{+-}^3 = 0.004$, and the temperature in terms of the reduced inverse temperature $\beta^* = 1/T^* = 4\pi k_B T\sigma_{+-}\varepsilon_0\varepsilon/e^2 = 8.6$ (we have taken for σ_{+-} the distance at which $g_{TBA-TPB}(\sigma_{+-}) = 1$, corresponding to 0.63 nm). The cluster size distribution of the RPM, at similar thermodynamics conditions, does feature a monotonic decay too (see ref.[31] and Figure 3). Only at lower temperatures, namely approaching the critical point of the RPM ($\beta^* = 20.4$[32]), the cluster size distribution function of this model changed significantly, adopting a "sawtooth" shape, which indicates that the ions in the RPM structure themselves preferentially into neutral clusters (see Figure 3). Assuming a similar behavior for the DCE and RPM solutions, it is clear that the coulombic interactions in the DCE solutions at experimentally relevant temperatures, are not strong enough to form preferentially neutral clusters.

We show in Figure 2 the TBA-DCE and TPB-DCE pair correlation functions. These were computed considering the center of mass distance between the DCE molecules and corresponding ion. DCE is more structured around the TPB than TBA as shown by the stronger oscillation in the former. The solvent can "penetrate" more into the TBA ion since this ion is less compact than TPB, which offers more steric hindrance for solvent penetration due to the bulky aromatic rings. These differences are also reflected in the solvation number (see Table 2), which is higher for TBA (between 9-11 DCE molecules) than TPB (between 7-9 DCE molecules). These numbers indicate that the organic ions are generally strongly solvated in the DCE solution. The solvation shell will therefore play an important role in determining the effective ion-ion interactions, which involve a large number of pair contributions between the atoms in the cations and anions. These interactions lead to inter-ionic van der Waals interactions that are much stronger than those experienced by simpler alkali halide ions. To test this idea we performed Brownian Dynamics (BD) simulation of the solution in an implicit solvent with a effective dielectric constant corresponding to that DCE at the specific ion concentration. These simulation results (not shown) in irreversible aggregation of the TBA and TPB ions, unlike what is observed in the simulations using explicit solvent. This BD simulations highlights the strength of the direct ion-ion dispersion interactions, and the important role of DCE in modulating these interactions.

Previous studies of simple aqueous solutions showed that depending on the strength of the Coulomb correlations the decay mode of these correlations is exponential (at low electrolyte concentration) or oscillatory (high electrolyte concentration). In alkali halide solutions the oscillatory decay mode is expected at high concentrations and low temperatures; the exponential decay has indeed been observed at low concentrations, 1 mM and 298 K. We have examined the transition from monotonic to oscillatory decay in the DCE solution, by computing the excess charge,

$$q_{exc}(r) = \pm 1 + (\pm n_{ii}(r) \mp n_{ij}(r)) \quad (1)$$

where n_{ij} is the running coordination number of particles of type

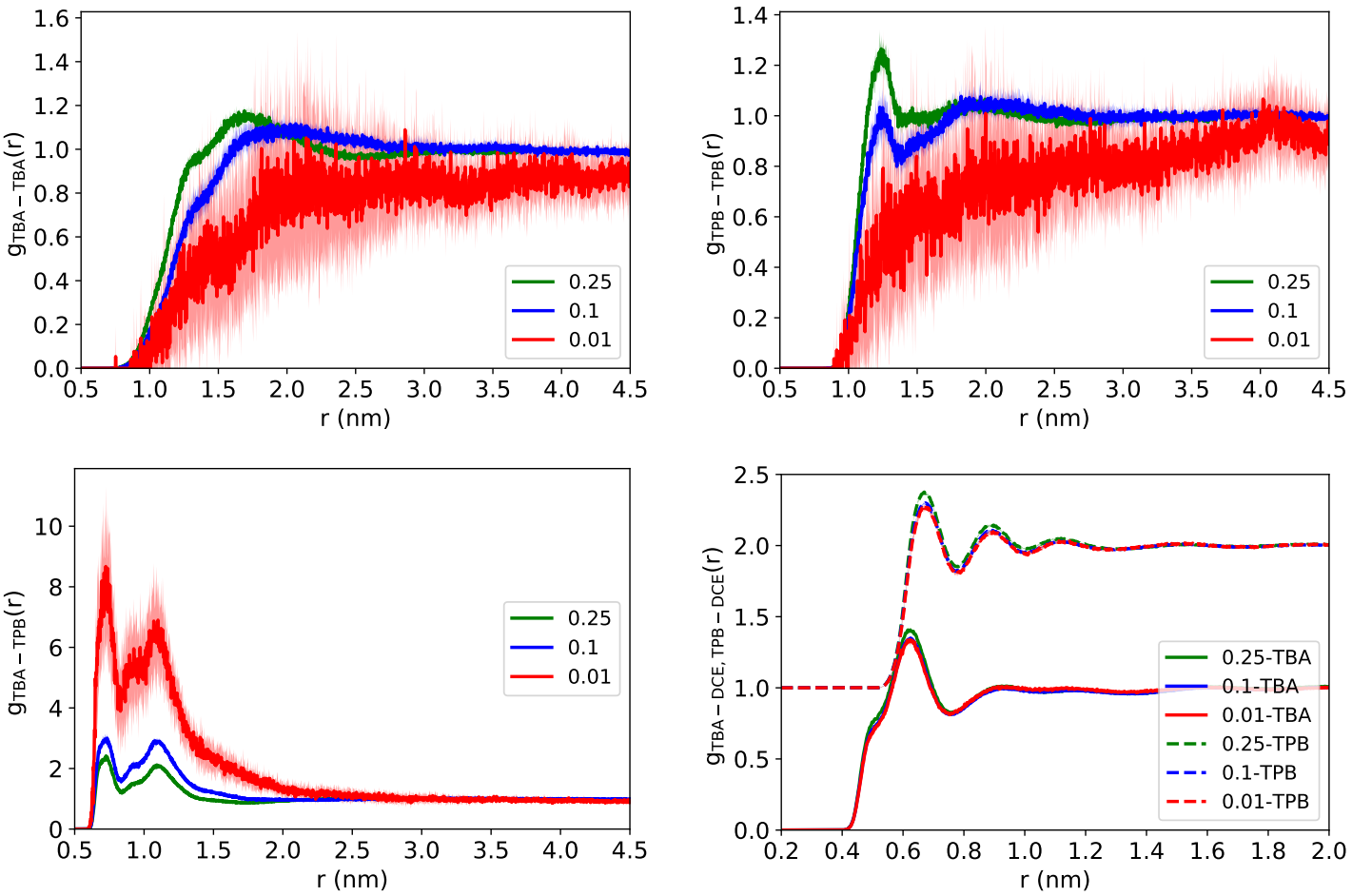

Fig. 2 Radial distribution functions (center-of-mass to center-of-mass) of TBA, TPB and DCE for the indicated concentrations. The radial distribution functions for the TPB-DCE case have been shifted upwards by one unit for clarity. The numbers in the insets indicate the concentration of salt in molal units. Top-left and Top-right panels from bottom to top: 0.01, 0.1 and 0.25 m. Bottom-left panel from bottom to top: 0.25, 0.1 and 0.01 m.

Table 2 Mean cluster size ($\langle S \rangle$), solvation number for TBA and TPB ions ($n_{TBA-DCE}$ and $n_{TPB-DCE}$), free energy of adsorption of the ions at the interface in k_BT units (β = 1/k_BT), and excess adsorption (ion/nm^2). The solvation number was obtained from the integral of the pair correlation function (see equation (2)), integrating up to the first minimum. Note that free energy calculations correspond to interfacial systems at concentrations $c_{int.}$, far from the interface.

c	$\langle S \rangle$	$n_{TBA-DCE}$	$n_{TPB-DCE}$	$c_{int.}$	$\beta\Delta F_{TBA}$	$\beta\Delta F_{TPB}$	Γ_{TBA}	Γ_{TPB}
0.01	1.1± 0.1	10.9± 0.1	8.8 ± 0.2	0.008	-1.53	-1.77	0.026±0.005	0.025±0.007
0.1	1.7±0.1	10.1± 0.1	8.3 ± 0.1	0.093	-0.74	-0.96	-0.026±0.030	-0.027±0.030
0.25	2.6±0.1	9.3 ± 0.1	7.5 ± 0.1	0.21	-1.06	-1.1	0.20±0.03	0.21±0.03

j surrounding a particle of type i, and the $\pm$ takes into account whether the central ion is the cation $+$ or anion $-$. The coordination number was obtained from the running integral,

$$n_{ij}(r) = 4\pi\rho_j \int_0^r r'^2 g_{ij}(r')dr', \qquad (2)$$

where ρ_j is the density of species j. We computed the coordination numbers by integrating the pair correlation functions with the radial distance defined by the distance between the center of mass of the ions. We show in Figure 4 the excess charge for anions (TPB) and cations (TBA). The excess charge decays monotonically at low concentrations, 0.01 m. Taking the distance at which the total charge, ± 1, is compensated by a factor of $1/e$ as indicative of the decay length of the electrostatic field, and taking into account the radial distance at which the charge starts to decay from ± 1, $r \sim 0.64$ nm, we get an effective decay length of the order of 1.5 nm. This result is reasonable, and close to the value one can infer from simple application of the Debye length formula using the average dielectric constant of DCE for the specific salt concentration, which gives, $\sim$1 nm for a concentration 0.01 m. The monotonic decay at low concentrations contrasts with the mechanism of charge compensation at higher concentrations, which features over-screening, as shown by the change in

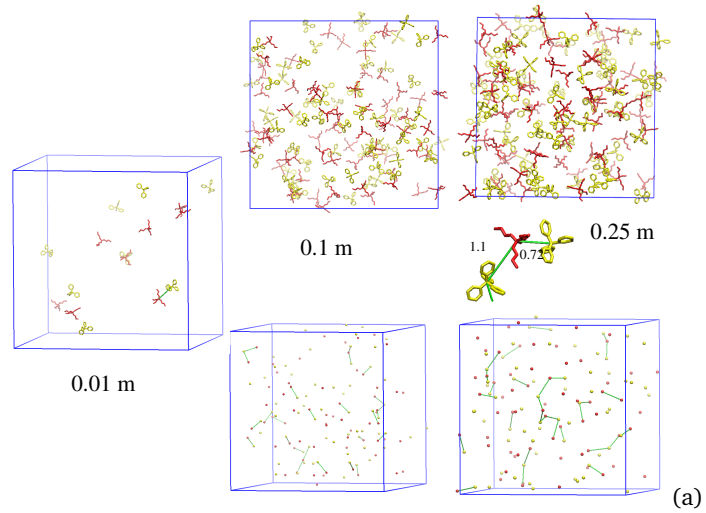

(a)

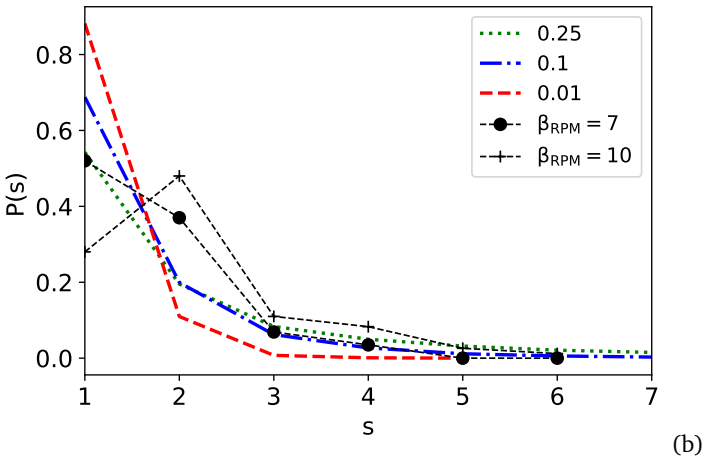

(b)

Fig. 3 (a) Snapshots of solutions at different concentrations, 0.01 m (left panel), 0.1 m (middle) and 0.25 m (right). TBA and TPB are shown in red and yellow, respectively. The green lines link ions that are part of the same cluster. The distance employed to construct the clusters corresponds to the second maximum in the TBA-TPB RDF, 1.1 nm. The additional snapshot for 0.25 m, features a trimer, TPB-TBA-TPB, highlighting the distances corresponding to the two maxima in $g_{TBA-TPB}(r)$, 0.72 and 1.1 nm (see Figure 2). (b) Cluster size distribution, $P(s)$, of DCE solutions for different molal concentrations, where s is the cluster size. The dashed lines and symbols represent the cluster size distribution of the Restricted Primitive Model at $\rho^* = 0.00727$ and two different inverse temperatures, $\beta^* = 7$ (circles) and $\beta^* = 10$ (crosses)[31].

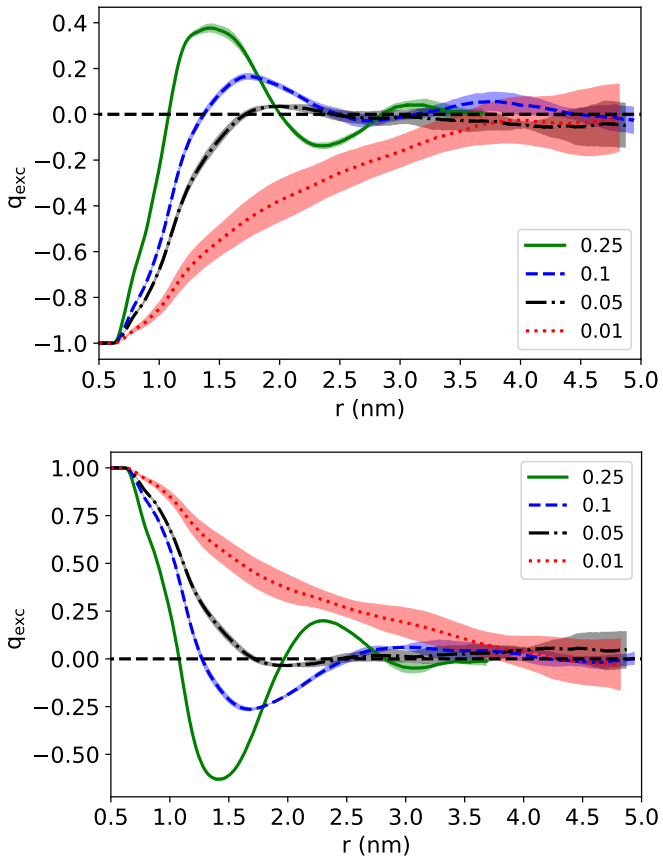

Fig. 4 Charge compensation as a function of radial distance for the tetraphenylborate anion (top) and the tetrabutylammonium cation (bottom). The shadowed areas indicate the uncertainty in the computed q_{exc}. The excess charges have been shifted by ± 1 to reflect the charge of the central ion and how this is compensated completely at long distances, $q_{exc} \to 0$.

sign of the charge at distances of the order of 1-2 nm, followed by an oscillatory decay. However, the charge never increases to values larger than the nominal charge of the cation or the anion.

Such oscillations have been observed before in aqueous solutions involving highly charged ions 2:2 (see *e.g.* ref.[29]). The theoretical foundations of the transition from monotonic to oscillatory profiles of the charge distribution around ions, with increasing electrolyte concentration have themselves a long history. Such effects in charge density correlation functions and screened potentials were first discussed as early as in 1936 by Kirkwood[33] in a standard primitive model of electrolytes. In the 1990s it was demonstrated by Kjellander and Mitchell using charge renormalization analysis[34], by Attard – for Ornstein-Zernike equation and for hypernetted chain approximation[35], and by de Carvalho and Evans[36] within the generalized mean spherical approximation of a restricted primitive model. Notably, very recently, Kjellander[37] published a detailed study of the onset of the oscillating mode of screening, correlating it with the effect of virtual clustering of ions of opposite sign. We note that the observation of over-screening in TBA-TPB-DCE solutions at much lower concentration than in aqueous solutions is clearly due again to the ∼8 times longer Bjerrum length in DCE than in water and simultaneously to the much stronger dielectric saturation effect. Indeed, for 0.25 m solution the average distance between ions is 1.5 nm, whereas the Bjerrum length in DCE is 5.6 nm. The Bjerrum length is a characteristic of comparison of electrostatic interaction between ions and the thermal energy. Because it is so large in DCE, the over-screening and ion-ion oscillation profiles emerge at substantially smaller concentrations of ions than in the aqueous solution, and so do the dielectric saturation effects.

3.2 Interfacial Properties

So far we have investigated the thermodynamic properties, structure and charge compensation of the DCE solutions in the bulk. The interfacial behavior of these solutions is of particular interest

in electrochemical experiments involving liquid-liquid interfaces. We performed computations of the liquid DCE/TBA-TPB-air interface, and quantified the degree of ion adsorption to the interface as well as the modification of the interfacial tension with salt concentration. We find that the surface tension increases in going from no salt to 0.01 m concentration. The increase is however small, and within the statistical significance of our computations. At higher concentrations the surface tension shows a significant reduction. Such dependence is opposite to the one observed in aqueous alkali halide solutions, where the surface tension increases, while a decrease has been reported in acid solutions, *e.g.* $HClO_4$, HNO_3 or HCl[38]. For alkali halides the effect can be interpreted in part due to the image force repulsion of ion charges from the dielectric-air interface, following the idea of Onsager-Samaras theory. For $HClO_4$, HNO_3 and HCl, image forces should be present too, but the fact that the surface tension decreases with concentrations highlights the importance of chemical effects, overruling the simple interpretation given by Onsager and Samaras. We note that adsorption of ionic surfactants at the water surface is well known, and that accumulation of ions has also been reported for the case of large anions, such as I^-, using rigid ion models[6], hence the adsorption of the large organic ions at the DCE surface is not surprising. To quantify the accumulation of ions at the DCE surface we performed additional simulations of DCE slabs containing difference concentrations of ions and computed the corresponding density profiles.

We show in Fig. 5 the density profiles of cations and anions relative to the interfacial plane (see vertical line in Fig. 5). The latter has been defined by fitting the total density profile to a hyperbolic tangent function, and the line corresponds to the location of the inflection point, which is generally taken in the case of pure fluids as the position of the equimolar dividing surface. We started our simulations from bulk solutions containing ions at 0.25, 0.1 and 0.01 m concentrations. As the simulation reaches the stationary state, some of the ions are adsorbed at the interface and the effective bulk concentration decreases (see horizontal line in Fig. 5). The final concentrations in the bulk region are indicated in the Figure caption and in Table 2.

The first conclusion from our simulations is that the ions have a strong tendency to accumulate at the interface, and the anions adsorb more strongly than the cations (see snapshots and density profiles in Figure 5). This behavior is consistent with the poorer solvation of the anion (see Table 2). Moreover, at the lowest concentration (see 0.008 m bulk concentration in Figure 5) there is a clear charge separation, with an adsorption peak corresponding to the cations lying further from the interface that the anion layer. This charge separation would lead to an effective interfacial potential drop. The charge separation disappears into the liquids, at about 3.5 nm from the DCE surface, and the solution recovers the electroneutrality (note that the density of cations and anions is equal within the error of the computations beyond that distance). Although the tendency to populate the interface is present at higher concentrations too, the charge separation is smaller. This result is consistent with the screening of the charge at higher concentrations. We used our simulations to quantify the degree of ion adsorption by calculating the interfacial free energy

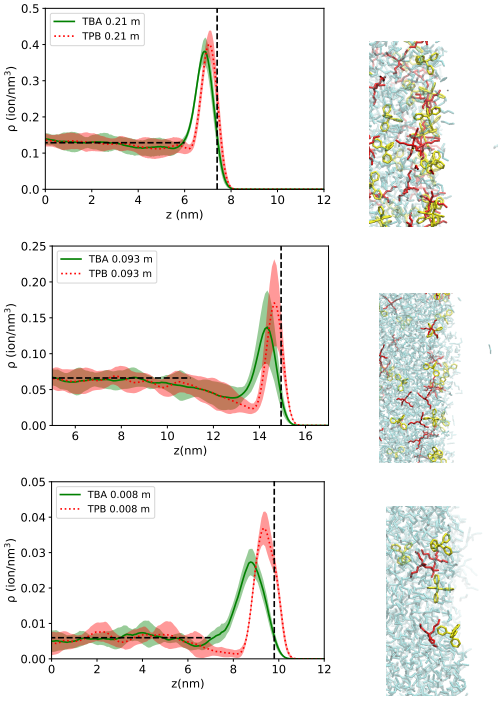

Fig. 5 Density profiles of cations and anions for DCE solution interfaces as a function of distance. The density profiles were obtained from simulations involving liquid slabs, and therefore two interfaces. The data represented in the figure were obtained from an average over both interfaces. The green and red shadowed areas represent the estimated scatter in the simulation data for the cations and anions, respectively. The horizontal and vertical dashed lines represent the bulk concentration and the location of the interface (Gibbs Dividing Surface, GDS), respectively. The GDS was calculated by fitting the total density profile to a hyperbolic tangent function.

of the ions at the DCE surface. The latter can be estimated using the reversible work theorem. From the ratio of the densities of the ions at the maximum of the adsorption peak and the density in the bulk we get for the cation (TBA) $\rho_{max}/\rho_b = 4.6$ (0.008 m), 2.1 (0.093 m), 2.9 (0.21 m), and for the anion (TPB) $\rho_{max}/\rho_b =$ 5.9 (0.008 m), 2.6(0.093 m), 3 (0.21 m). These data lead to the adsorption free energies, $\Delta F/k_BT = F_{int} - F_{bulk} = -\ln(\rho_{max}/\rho_b)$, compiled in Table 2. The data clearly show the stabilization of the ions at the interface, with relatively high free energies at the lowest concentrations.

It is instructive to compare this free energy with the one that would be obtained from adsorption of a sphere with a radius of 0.5 nm, similar to TPB. This free energy assuming a $\pi/2$ contact angle would be (using the surface tension corresponding to 0.01 m, see Table 1), $\Delta F_{capillary} = -\pi R^2 \gamma_{DCE} \sim 7$ k_BT. This value is higher than the one reported in Table 2, but we note that the TPB ion is immersed mostly in the DCE phase (see maximum in the density profile and location of the interface). We can address this by considering the contact angle. which can be estimated from the immersion of the ion in the DCE phase, h, namely, the difference between the maximum in the density profile of TPB and the position of the interface (see dashed vertical line in Figure 5), so that $\cos\theta = h \sim 0.94$ for $R = 0.5$ nm and $\Delta F_{capillary} =$

$-\pi R^2 \gamma_{DCE}(1-\cos\theta)^2 \sim 0.03$ k$_B$T. This value is admittedly too low, highlighting the limitation of the capillary approach to predict precise estimates of the adsorption energies of such entities as the organic TPB ions (whereas this approach works fairly well already for small nanoparticles[39,40]). A similar exercise for the other two concentrations (accounting for the different surface tensions, see Table 1) gives, $\cos\theta_{0.093} \sim 0.6$ and $\Delta F_{capillary,0.093\ m} \approx -1.0$ k$_B$T, and $\cos\theta_{0.21\ m} \sim 0.6$ and $\Delta F_{capillary,0.21\ m} \approx -0.7$ k$_B$T, in much better agreement, notwithstanding the precision issues mentioned above. We note that the capillary calculation above should be taken with care since the macroscopic considerations might not apply directly to the organic ions, also because they are not exactly spherical.

We have shown that the simulations predict significant accumulation of ions at the DCE surface, with the TPB ions protruding more towards the vapor phase. We have estimated the adsorption, *i.e.* the number of ions per unit area using,

$$\Gamma_i = \int_{z_0}^{z_M} \left(\rho_i(z) - \rho_{i,l}\right) dz + \int_{z_M}^{z_1} \left(\rho_i - \rho_{i,v}\right)(z) dz \qquad (3)$$

where we set $z_0 = 0$ (the middle of the liquid slab), $z_1 = 17$ nm (in the vapor region, see Figure 5), and z_M is the position of the Gibbs Dividing Surface (see vertical dashed line in Figure 5), which was obtained from the analysis of the density profile of the solvent (DCE). $\rho_i(z)$ is the density of ions of type i at position z, and $\rho_{i,l}$ and $\rho_{i,l} \equiv 0$ are the densities of the ions in the liquid (see horizontal dashed line in Figure 5) and vapor bulk phases, respectively. We have collected in Table 2 the results from this calculation. The adsorption at the interface at the lower concentrations is relatively low, this is despite the prominent density peaks. At the lower concentrations the density peaks are followed by depletion regions which reduce significantly the final value of the adsorption. The importance of these depletion regions has been highlighted before in experimental studies of alkali halides, where despite prominent ion accumulation, the net adsorption is still negative (see ref. [7]). The uncertainty in the adsorption at low concentrations is relatively high, which limits our ability to estimate accurately the adsorption in this regime. At high concentrations > 0.2 m the precision is much better and a clear trend for positive adsorption is evident. The adsorption amounts to $\sim$0.2 e/nm^2 ($\sim 3\ \mu$C/cm^2) for each ion. This estimate is of the order of the interfacial excess charge reported in experimental studies of DCE-water interfaces[15]. It is also close to the value that can be obtained from the Gibbs adsorption isotherm (GAI),

$$d\gamma = -\sum_i \Gamma_i d\mu_i \approx= -\Gamma RT d\ln c \qquad (4)$$

where $\Gamma = \Gamma_+ + \Gamma_-$ is the total adsorption due to cations and anions, and c is the electrolyte concentration in the bulk. Using a finite difference version equation (4) for the ideal case, $\Gamma = -(c\,RT)(\Delta\gamma/\Delta c)$, where R is the gas constant, and the surface tension values in Table 1 for concentrations 0.1 and 0.25 m, we get $\Gamma \sim 0.2$ ions/nm^2 for $c = 0.175$ m, which is of the order but lower than the simulation result for $\Gamma = 0.41$ ions/nm^2 at c =0.21 m. The deviation can be connected to the different concentration and also to the relevance on non ideal effects connected to ion-ion interactions. Despite this, the analysis in terms of the GAI and existing experimental data, demonstrate that the adsorption obtained with our model is within the expected range.

Our simulations show an enhancement of the density of cations and anions at the interface, with a relative shift of the density peak for the latter towards the vapor phase. This local charge separation should lead to an interfacial dipole and to a shift of the electrostatic interfacial potential of the pristine DCE interface. We have quantified this shift by computing the mean electrostatic potential, $V(z)$, using Gauss' theorem,

$$V(z'') = \frac{-1}{\varepsilon_0} \int_0^z dz' \int_0^{z'} \rho_q(z'') dz'' \qquad (5)$$

where $\rho_q(z) = \sum_{i=1}^{N} \delta(z - z_i) q_i / A$ is the charge density at position z, and A the cross sectional area of the simulation box. The sum runs over all the charges in the system, namely, TBA$^+$ and TPB$^-$ ions, and DCE molecules. We have represented in Figure 6 both the total electrostatic potential using all the charges due to the solvent and ions, and also the individual contributions, namely, from ions and solvent, to the total potential. The electrostatic potential of pure DCE is +0.25 V, revealing a strong reorientation of the molecular at the interface. This potential can be compared with the electrostatic potential of state of the art water models (e.g. SPC/E), with values of the order of -0.5 V.

The accumulation of ions at the surface results in a significant upward shift in the total electrostatic potential, ~ 0.25 V in going from pure DCE to the highest concentration, 0.21 m. This shift is connected to the field generated by the ions and the concomitant polarization of DCE, whose field changes sign upon adding salt (see Figure 6). The modification of the electrostatic potential has been noted before in alkali halide solutions in water at higher concentrations, although in this case the total electrostatic potential varied little with respect to that of pure water[6]. The strong modification of the total electrostatic potential represents a distinctive feature of the organic ions studied here. We find that the solvent contribution changes significantly with concentration, even reversing the sign, which indicates a strong reorientation of the DCE interfacial molecules. The reorientation is induced by the organic ions accumulated at the interface. Whereas at liquid/liquid interfaces (water/DCE) the magnitude of the this potential shift can be different, a similar effect can be expected there, as well. This will cause a shift in the potential of zero charge with respect to a case where ion adsorption is not present.

4 Conclusions

We have performed an atomistic molecular dynamics simulation of tetrabutylammonium (TBA) and tetraphenylborate (TPB) ions dissolved in dichloroethane (DCE), and we have investigated the solvation structure and ion correlations in bulk and at interfaces. The model reproduces well existing experimental measurements of dielectric constant, ion diffusion coefficients and surface tension. We conclude the following from the analysis of our simulations.

• Although our model predicts a decrease of dielectric constant with increasing salt concentration, as observed in experiments of

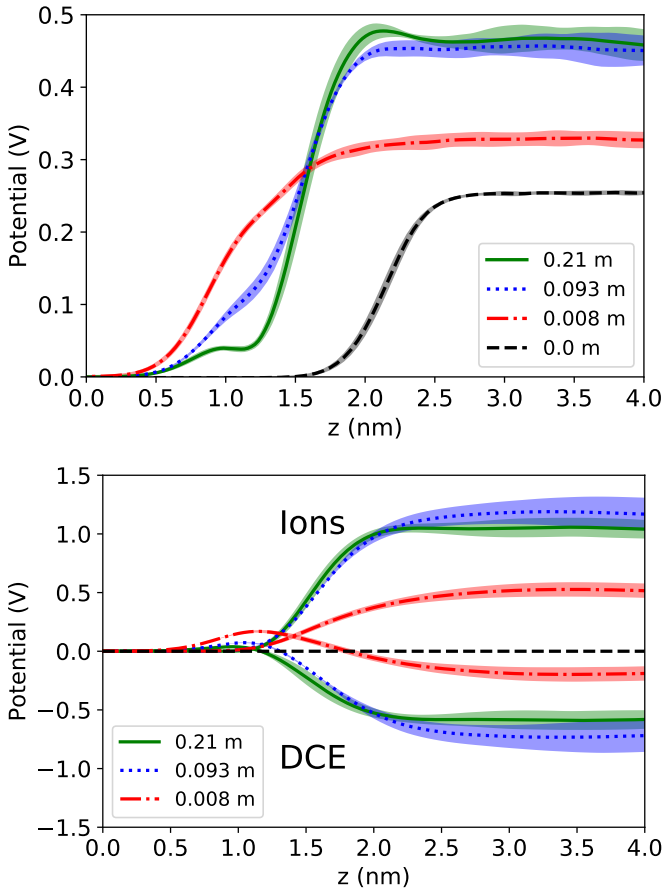

Fig. 6 (Top) Total electrostatic potential of the DCE-TBA-TPB interfaces as a function of the salt concentration. (Bottom) Ionic and solvent contributions to the total electrostatic potential. Taking z=3 nm as a reference, a positive electrostatic potential (> 0) corresponds to the ions and the negative one (< 0) to DCE.

alkali halides, other properties change differently. In particular, the density of the solution decreases with increasing concentration, and the surface tension of DCE decreases too. These trends denote key differences with respect to strongly hydrated smaller alkali ions. The decrease in the surface tension is driven by the accumulation of ions at the interface. This observation disagrees with the classical view of Onsger-Samaras theory, where a depletion of ions from the interface should be observed based on image charge repulsion of the ions from the interface. Large organic ions seemingly possess some surfactant properties that dominate over image-charge repulsions. The molecular structure of the ions is therefore important.

• We observe a change in the mechanism of charge compensation in the interval of concentration 10-100 mm. At low concentrations, the charge compensation decays monotonically. This observation is consistent with mean field behavior observed in experimental studies of immiscible electrolytic solutions, which can be described accurately using the Verwey-Niessen theory. However, at the higher concentrations the charge compensation features an oscillatory behavior, characteristic of dense ionic systems, with evident over-screening effects. We estimate that transition from the monotonic to the oscillatory decay occurs at concentration ~ 0.02 m. This behavior is fairly different to the one observed in 1:1 alkali halide solutions in water, where such transition is not observed even at concentrations as high as 1 molal. The differences between these two electrolytes are likely connected to the lower dielectric constant of the DCE as compared with water (eight times smaller and eight times longer Bjerrum length).

• The ionic correlations become evident at high concentrations > 0.1 m, with the ions forming a significant number of "Bjerrum" dimers, $\sim$ 20%, as well as smaller proportion of larger clusters. Such clusters are readily observed in our simulations.

• TBA is, generally, more strongly solvated (9-11 DCE molecules), than TPB (7-9 DCE molecules). The different solvation is reflected in the interfacial behavior of these two ions. TPB protrudes more towards the vapor phase than TBA, which adsorbs just below the TPB layers at the DCE surface. The simulation show accumulation of ions at the interface, as well as clustering, and the characteristic adsorption energy relative to the DCE liquid is of the order of -1.5 to -1 k_BT units, with the larger values corresponding to the anion (TPB).

• The adsorption at higher concentrations, 0.21 m, reaches values of ~ 0.25 ions/nm^2, while for concentrations typical of electrochemical experiments at liquid-liquid interfaces, $\sim$ 10 mm, is ~ 0.03 ions/nm^2. The accumulation of ions is shown to have an important effect on the interfacial electrostatic potential, with significant changes of ~ 0.25 V in going from pure DCE to solutions at 0.21 m. The shift in the electrostatic potential is much larger than the one reported for alkali halide solutions. This can be rationalized by the strong accumulation of the ions at the interface, still different for cations and anions, which is likely induced by the large ion size and a weaker solvophilicity.

This work is a first step towards a detailed molecular level understanding of the properties of organic ions in organic polar solvents used in electrochemical experiments. In addition to providing answers to fundamental questions concerned with the electrostatic properties of these solutions, our work should serve a reference for future studies involving liquid-liquid interfaces, such as the ones employed in ITIES. This topic will be the focus of future works.

Conflicts of interest

There are no conflicts to declare.

Acknowledgements

We acknowledge the award of a Research Grant by The Leverhulme Trust (RPG-2016-223) and the EPSRC for a PhD bursary to OR. We thank the Imperial College High Performance Computing Service for providing computational resources.

Notes and references

1 Y. Levin, *Rep. Prog. Phys.*, 2002, **65**, 1577 – 1632.
2 L. Onsager and N. N. T. Samaras, *The Journal of Chemical Physics*, 1934, **2**, 528–536.
3 Y. Levin, *The Journal of Chemical Physics*, 2000, **113**, 9772–9775.

4 P. Jungwirth and D. J. Tobias, *Chemical Reviews*, 2006, **106**, 1259–1281.

5 Y. Levin, A. P. dos Santos and A. Diehl, *Phys. Rev. Lett.*, 2009, **103**, 257802.

6 F. Bresme, E. Chacón, P. Tarazona and A. Wynveen, *The Journal of Chemical Physics*, 2012, **137**, 114706.

7 P. B. Petersen and R. J. Saykally, *Annual Review of Physical Chemistry*, 2006, **57**, 333–364.

8 A. A. Lee, C. S. Perez-Martinez, A. M. Smith and S. Perkin, *Faraday Discuss.*, 2017, **199**, 239–259.

9 L. M. Varela, M. García and V. Mosquera, *Physics Reports*, 2003, **382**, 1.

10 Z. Samec, *Chemical Reviews*, 1988, **88**, 617–632.

11 H. Girault and D. Schiffrin, *Electroanalytical Chemistry*, 1989, **15**, 1 – 141.

12 Y. Montelongo, D. Sikdar, Y. Ma, A. McIntosh, L. Velleman, A. Kucernak, J. Edel and A. Kornyshev, *Nature materials*, 2017, **16**, 1127–1135.

13 J. B. Edel, A. A. Kornyshev, A. R. Kucernak and M. Urbakh, *Chem. Soc. Rev.*, 2016, **45**, 1581–1596.

14 M. D. Scanlon, E. Smirnov, T. J. Stockmann and P. Peljo, *Chemical Reviews*, 2018, **118**, 3722–3751.

15 B. Hou, N. Laanait, H. Yu, W. Bu, J. Yoon, B. Lin, M. Meron, G. Luo, P. Vanysek and M. L. Schlossman, *The Journal of Physical Chemistry B*, 2013, **117**, 5365–5378.

16 G. Bussi, D. Donadio and M. Parrinello, *The Journal of Chemical Physics*, 2007, **126**, 014101.

17 H. J. C. Berendsen, J. P. M. Postma, W. F. van Gunsteren, A. DiNola and J. R. Haak, *The Journal of Chemical Physics*, 1984, **81**, 3684–3690.

18 U. Essmann, L. Perera, M. L. Berkowitz, T. Darden, H. Lee and L. G. Pedersen, *The Journal of Chemical Physics*, 1995, **103**, 8577–8593.

19 W. L. Jorgensen and J. Tirado-Rives, *Journal of the American Chemical Society*, 1988, **110**, 1657–1666.

20 A. K. Malde, L. Zuo, M. Breeze, M. Stroet, D. Poger, P. C. Nair, C. Oostenbrink and A. E. Mark, *Journal of Chemical Theory and Computation*, 2011, **7**, 4026–4037.

21 O. Chris, V. Alessandra, M. A. E. and V. G. W. F., *Journal of Computational Chemistry*, **25**, 1656–1676.

22 H. Berendsen, D. van der Spoel and R. van Drunen, *Computer Physics Communications*, 1995, **91**, 43 – 56.

23 K. Nörtemann, J. Hilland and U. Kaatze, *The Journal of Physical Chemistry A*, 1997, **101**, 6864–6869.

24 X. Duan and I. Nakamura, *Soft Matter*, 2015, **11**, 3566–3571.

25 A. Levy, D. Andelman and H. Orland, *The Journal of Chemical Physics*, 2013, **139**, 164909.

26 I. Nakamura, *The Journal of Physical Chemistry B*, 2018, **122**, 6064–6071.

27 Y. Marcus, *The Properties of Solvents: Wiley*, 1998.

28 A. K. Kontturi, K. Kontturi, J. A. Manzanares, S. Mafé and L. Murtomäki, *Berichte der Bunsengesellschaft für physikalische Chemie*, **99**, 1131–1136.

29 J. Abascal, F. Bresme and P. Turq, *Molecular Physics*, 1994, **81**, 143–156.

30 A. Volkov, D. Deamer, D. Tanelian and V. Markin, *Progress in Surface Science*, 1996, **53**, 1 – 134.

31 F. Bresme, E. Lomba, J. J. Weis and J. L. F. Abascal, *Phys. Rev. E*, 1995, **51**, 289–296.

32 A. Z. Panagiotopoulos, *The Journal of Chemical Physics*, 2002, **116**, 3007–3011.

33 J. G. Kirkwood, *Chemical Reviews*, 1936, **19**, 275–307.

34 R. Kjellander and D. Mitchell, *Chemical Physics Letters*, 1992, **200**, 76 – 82.

35 P. Attard, *Phys. Rev. E*, 1993, **48**, 3604–3621.

36 R. L. de Carvalho and R. Evans, *Molecular Physics*, 1994, **83**, 619–654.

37 R. Kjellander, *The Journal of Chemical Physics*, 2018, **148**, 193701.

38 P. K. Weissenborn and R. J. Pugh, *Journal of Colloid and Interface Science*, 1996, **184**, 550 – 563.

39 F. Bresme and M. Oettel, *Journal of Physics: Condensed Matter*, 2007, **19**, 413101.

40 M. E. Flatté, A. A. Kornyshev and M. Urbakh, *Journal of Physics: Condensed Matter*, 2008, **20**, 073102.